

This work was written as part of one of the author's official duties as an Employee of the United States Government and is therefore a work of the United States Government. In accordance with 17 U.S.C. 105, no copyright protection is available for such works under U.S. Law.

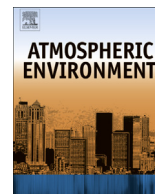
Public Domain Mark 1.0

<https://creativecommons.org/publicdomain/mark/1.0/>

Access to this work was provided by the University of Maryland, Baltimore County (UMBC) ScholarWorks@UMBC digital repository on the Maryland Shared Open Access (MD-SOAR) platform.

Please provide feedback

Please support the ScholarWorks@UMBC repository by emailing scholarworks-group@umbc.edu and telling us what having access to this work means to you and why it's important to you. Thank you.



Characterization of aerosols over the Indochina peninsula from satellite-surface observations during biomass burning pre-monsoon season

Ritesh Gautam^{a,b,*}, N. Christina Hsu^b, Thomas F. Eck^{a,b}, Brent N. Holben^b, Serm Janjai^c, Treenuch Jantarach^c, Si-Chee Tsay^b, William K. Lau^b

^a GEAR/Universities Space Research Association, Columbia, MD 21044, USA

^b NASA Goddard Space Flight Center, Greenbelt, MD 20771, USA

^c Silpakorn University, Nakhon Pathom 73000, Thailand

HIGHLIGHTS

- Characterization of aerosols over Indochina from satellite and surface observations.
- Multi-year analysis of aerosol vertical distribution is presented from CALIOP data.
- Regional aerosol loading is found to be significantly absorbing from AERONET data.
- The smoke-laden aerosol loading is found to exhibit a significant diurnal pattern.
- Satellite-based aerosol radiative impact is assessed using CERES data.

ARTICLE INFO

Article history:

Received 26 December 2011

Received in revised form

4 May 2012

Accepted 5 May 2012

Keywords:

Aerosol
Remote sensing
Southeast Asia
Biomass burning

ABSTRACT

This paper presents characterization of aerosols over the Indochina peninsular regions of Southeast Asia during pre-monsoon season from satellite and ground-based radiometric observations. Our analysis focuses on the seasonal peak period in aerosol loading and biomass burning, prior to the onset of the Asian summer monsoon, as observed in the inter-annual variations of Aerosol Optical Depth (AOD) and fire count data from MODIS. Multi-year (2007–2011) analysis of spaceborne lidar measurements, from CALIOP, indicates presence of aerosols mostly within boundary layer, however extending to elevated altitudes to ~4 km over northern regions of Indochina, encompassing Myanmar, northern Thailand and southern China. In addition, a strong gradient in aerosol loading and vertical distribution is observed from the relatively clean equatorial conditions to heavy smoke-laden northern regions (greater aerosol extinction and smaller depolarization ratio). Based on column-integrated ground-based measurements from four AERONET locations distributed over Thailand, the regional aerosol loading is found to be significantly absorbing with spectral single scattering albedo (SSA) below 0.91 ± 0.02 in the 440–1020 nm range, with lowest seasonal mean SSA (most absorbing aerosol) over the northern location of Chiang Mai (SSA ~ 0.85) during pre-monsoon season. The smoke-laden aerosol loading is found to exhibit a significant diurnal pattern with higher AOD departures during early morning observations relative to late afternoon conditions (peak difference of more than 15% amplitude). Finally, satellite-based aerosol radiative impact is assessed using CERES shortwave Top-of-Atmosphere flux, in conjunction with MODIS AOD. Overall, a consistency in the aerosol-induced solar absorption characteristic is found among selected regions from ground-based sunphotometer-derived spectral SSA retrievals and satellite-based radiative forcing analysis.

© 2012 Elsevier Ltd. All rights reserved.

1. Introduction

The Indochina peninsular regions in Southeast Asia witness intense seasonal biomass burning in the form of wildland forest

fires as well as agricultural crop burning and forest conversion fires during the boreal spring. Aerosol concentrations during the pre-monsoon season (March–April) are typically at peak associated with biomass burning activity and contribute significantly to the regional emissions (Carmichael et al., 2003; Janjai et al., 2009; Streets et al., 2009). The seasonal emissions peak occurs prior to the onset of the Asian summer monsoon rains and is prevalent over the

* Corresponding author. GEAR/Universities Space Research Association, Columbia, MD 21044, USA.

E-mail address: ritesh.gautam@nasa.gov (R. Gautam).

forested regions of the peninsula including Myanmar and northern Thailand. Smoke plumes due to biomass burning, accompanied by anthropogenic emissions, result in dense haze conditions, with episodic pollution levels at surface (e.g., PM₁₀, Total Suspended Particulate, etc) far exceeding the regional air quality standards during the pre-monsoon season (Chew et al., 2008; Pengchai et al., 2009). In addition to air quality effects, aerosols from this region, mostly fine-mode smoke plumes, have been shown to have potential climate impacts by altering cloud microphysics (Ramanathan et al., 2001) and perturbing regional radiation budget (Hsu et al., 2003) during pre-monsoon season.

In terms of large-scale climatology, importance of the Indochina peninsula is well recognized as this region experiences the earliest rainfall spells in Asia signaling the onset of the summer monsoon. Onset of the monsoon typically occurs during late April–early May associated with enhanced convective activity over Indochina peninsula and southern Bay of Bengal (Lau and Yang, 1997). During the dry pre-monsoon season, aerosol solar absorption plays a vital role, with potential implications in perturbing the summer monsoon circulation, regional rainfall patterns and long-term trends, and thus the overall hydrological cycle of the Asian regions, via radiative–convective processes (Ramanathan et al., 2005; Lau et al., 2006). Specifically over the Indochina peninsula, aerosol radiative effect becomes more important as smoke plumes have been observed to advect over stratiform clouds, in turn leading to enhanced solar absorption above clouds during the stable pre-monsoon conditions (Hsu et al., 2003). In general, prior to the monsoon onset period, a stable and widespread inversion layer prevails over the inland regions of Indochina peninsula including Thailand, Vietnam, Laos and Southern China (Nodzu et al., 2006). The strong inversion layer, most pronounced near-surface and in lower troposphere, develops during the dry winter season and persists through March–April, as shown by long-term radiosonde observations, before significantly weakening during May through September, due to enhanced convection and onset of the rainy period. During the pre-monsoon period, the enhanced near-surface inversion and capping of pollutants in the boundary layer results in hazy conditions over the Indochina region – often visible in satellite imagery (Fig. 1a).

In the context of the potential role of pre-monsoon aerosol loading in perturbing radiative energy balance and regional hydrological cycle, this paper focuses on aerosol characterization over the Indochina peninsula from an observational satellite–surface radiometric perspective. Inter-annual variability of the regional aerosol loading is studied from satellite (MODIS) data in relation with the enhanced pre-monsoon biomass burning activity. Regional aerosol vertical distribution is also studied over the northern and southern regions of the Indochina peninsula from multi-year analysis of spaceborne lidar (CALIOP) aerosol extinction measurements. Aerosol optical properties (optical depth, volume size distribution, and Single Scattering Albedo) are examined over a number of locations in Thailand using the AERONET ground-based sunphotometer observations. Strongly related to the regional meteorology, the pre-monsoon smoke-laden aerosol loading is further analyzed in terms of daytime variability. Overall, the present study aims to provide insight into the regional aerosol distribution in terms of optical/radiative properties, daytime variability, vertical distribution and radiative effect.

2. Datasets

2.1. AERONET retrieved aerosol optical properties

Version 2 retrievals of aerosol optical properties measured from CIMEL sunphotometers over Thailand (in the form of

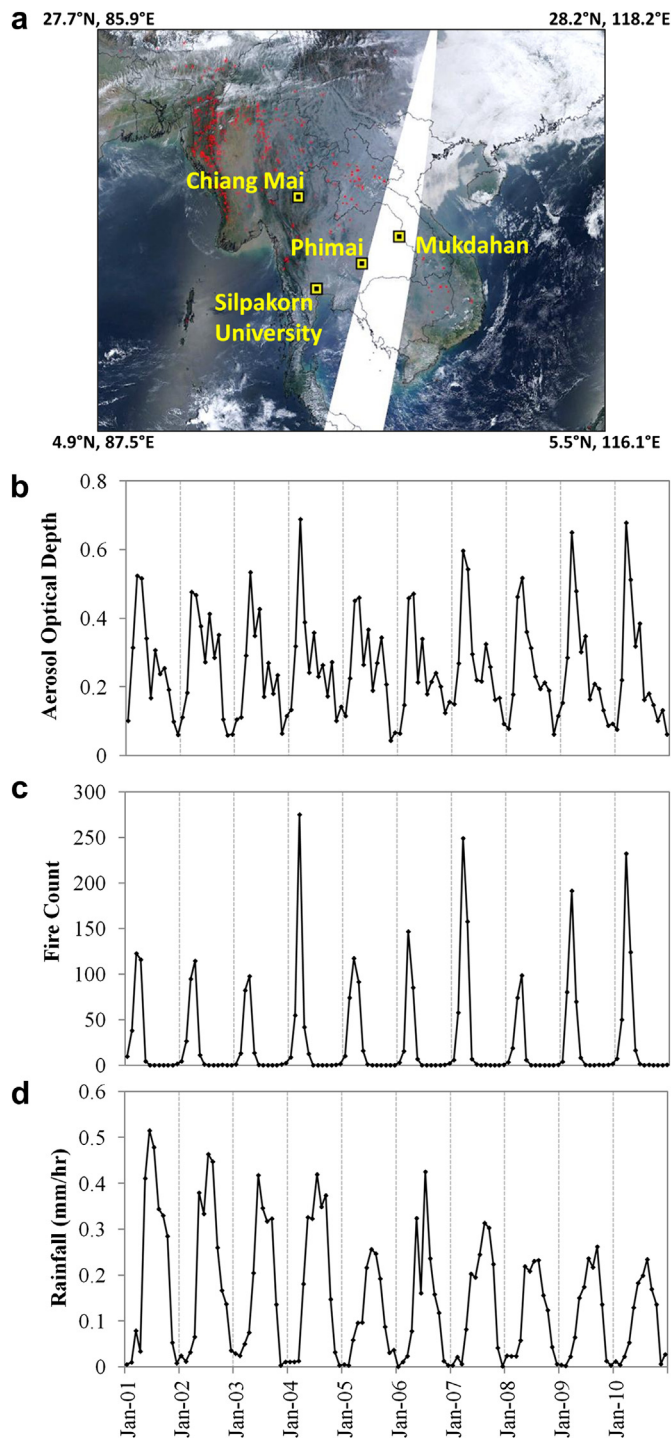


Fig. 1. (a) Location of AERONET sites for which data are used in this paper with background Terra/MODIS image on March 13, 2010 showing smoke-laden Indochina peninsula. MODIS-detected fires prevalent in Myanmar and northern Thailand are shown in red. Inter-annual variability of (b) MODIS AOD, (c) MODIS fire count, and (d) TRMM rainfall (mm hr⁻¹) from 2001 to 2010, averaged over 92°–104°E and 18°–24°N, representing the northern region of Thailand and Myanmar. (For interpretation of the references to color in this figure legend, the reader is referred to the web version of this article.)

quality assured Level-2 data), part of the Aerosol Robotic Network (AERONET) project (Holben et al., 1998), are used in this paper. The direct sun radiometric measurements are made at eight spectral channels (340–1020 nm) and sky radiance

measurements at four spectral channels (440, 670, 870 and 1020 nm). Water vapor content in the atmosphere is retrieved from the direct measurements at the 940-nm channel, and aerosol optical depth (AOD) data are retrieved at the remaining seven channels. AOD is measured with high accuracy ~ 0.01 in the visible and near-infrared wavelength and ~ 0.02 in the ultraviolet (Eck et al., 1999). The CIMEL sky radiance measurements in conjunction with the direct sun measurements of optical depths are used to retrieve optical equivalent aerosol volume size distributions (ASD) and refractive indices and hence deduce the spectral dependence of single scattering albedo (SSA).

2.2. MODIS aerosol optical depth and fire count

Collection 5 Terra/MODIS AOD data, along with MODIS-derived fire count activity information, were used to study the inter-annual variability of aerosol loading in relation with the enhanced pre-monsoon biomass burning activity (Levy et al., 2007). Globally gridded monthly mean MODIS products, with spatial resolution of $1^\circ \times 1^\circ$ were obtained for the period 2001–2010 from the NASA LAADS web portal.

2.3. CALIOP data

This study also uses observations from CALIOP that provide global vertically resolved measurements of atmospheric aerosols. With its capability of depolarization measurements, CALIOP can also distinguish dust from other types of aerosols (Liu et al., 2008). We use the Level 2 (version 3.01) profile product consisting of aerosol extinction and volume depolarization ratio (VDR) of the detected aerosol layers. The VDR derived from CALIOP backscatter measurements (Liu et al., 2008), is indicative of the type of particulates and can be effectively used to discriminate spherical (such as sulfate) with non-spherical (such as dust) aerosols. The VDR is defined as the ratio of the perpendicular and parallel components of the attenuated backscatter signal. Level-2 CALIOP extinction coefficient profiles are also used to characterize vertical aerosol loading. The prelaunch goal of the CALIPSO mission was to retrieve aerosol extinction coefficients accurate to within $\pm 40\%$ (Winker et al., 2010). Only night-time aerosol retrievals are shown here from CALIOP, because measurements during daytime are affected by greater noise associated with enhanced convection.

2.4. CERES Top-of-Atmosphere shortwave flux

In order to understand the effect of aerosols on the radiant energy flux, we use the TOA flux observations from the spaceborne CERES instrument. The CERES provides broadband radiance measurements at the TOA, both in the longwave and shortwave (Wielicki et al., 1996). We use the Single Scanner Footprint (SSF) data product (Edition 3A) that contains aerosol and cloud properties from the MODIS for each CERES footprint and reports measured TOA radiances, which are converted to fluxes using angular distribution models derived from CERES radiance measurements (Loeb and Kato, 2002). The best estimate of the error in CERES TOA flux due to the radiance-to-flux conversion is 3% (10 W m^{-2}) in the shortwave (SW). The overall bias in regional monthly mean SW TOA flux is less than 0.2 W m^{-2} and the regional RMS error ranges from 0.70 to 1.4 W m^{-2} . In this study, we use the daily SW flux data product with spatial resolution of $\sim 20 \text{ km}$ at nadir for a period of two years (2008 and 2009) covering the pre-monsoon period February–April.

3. Results and discussion

3.1. Inter-annual variability of aerosol loading

Aerosol loading over the Indochina peninsula varies depending on the timing of the rainy season and thus follows a strong seasonal cycle. For example, over Thailand, there are two peaks in the monsoon rainfall season namely in May and August/September associated with southwesterly (typical to the Asian monsoon) and northeasterly flow (reversal of the monsoon), respectively. The southwesterly wind flow is enriched with moist air from the northern Indian Ocean toward the inland regions and is blocked by the elevated mountain ranges in Myanmar causing heavy precipitation over Thailand. Fig. 1 shows the inter-annual variability of MODIS AOD over the northern southeast Asia region ($92^\circ\text{--}104^\circ\text{E}$, $18^\circ\text{--}24^\circ\text{N}$) along with the MODIS-detected fire activity (represented by fire pixel counts). The yearly AOD starts to build up from January–February and typically peaks during March–April with highest monthly mean values above 0.5 during the extended dry season. With the onset of the monsoon, the aerosol loading significantly diminishes and further continues to drop from May–June onwards. Post-monsoon marks the beginning of the dry season when agricultural crop burning is prevalent as well as intense forest fires in the mountainous regions, along the Thai–Myanmar border, resulting in fine-mode dominated haze. The MODIS-detected fire activity also peaks during the February–April period and is well-correlated ($r^2 = 0.66$) with the peak AOD period on an inter-annual basis (see supplementary Fig. S1), suggesting smoke due to forest fire/crop burning as a major cause of the seasonal peak in the AOD.

3.2. Aerosol vertical distribution

The aerosol vertical distribution over the Indochina peninsula region is studied using CALIOP aerosol extinction profiles during the pre-monsoon season, February–April, for a 5-year period from 2007 to 2011. CALIOP data for this period were obtained over the study region covering the domain of $5^\circ\text{--}25^\circ\text{N}$ and $90^\circ\text{--}110^\circ\text{E}$ (Fig. 2a). A total of 608 CALIOP tracks were available for the analysis with each transect line (blue), in Fig. 2a, representing about 40 tracks. Aerosol extinction (σ) profiles were screened by fixing a threshold ($\sigma > 0.7 \text{ km}^{-1}$), above which data were filtered out, in order to minimize any residual cloud contamination due to potential artifacts and/or aerosol near cloud cases. This screening may possibly reject heavy aerosol loading events from our analysis, however it allows us to avoid potential artifacts and therefore reduce biases in the vertical characterization. Post data filtering and processing, the CALIOP data were averaged to represent zonal mean aerosol extinction profile from 5°N to 25°N i.e., from the equatorial Bay of Bengal and South China Sea regions to northern Thailand, Myanmar and southern China (Fig. 2b). A spatial gradient in the aerosol loading and vertical extent is clearly observed from the relatively clean oceanic regions to the northern polluted land areas, with σ generally less than 0.07 km^{-1} and greater than 0.15 km^{-1} , respectively. Over the oceanic region, there is little indication of a prominent aerosol layer suggesting relatively clean maritime conditions (a uniform peak at $\sim 0.6 \text{ km}$ asl is observed between 5° and 10°N that is associated with local aerosol emissions over the Sumatra islands). Fig. 3 also provides a more clear representation of the zonal mean distribution with aerosols extending up to 4 km over the northern land areas ($15^\circ\text{--}25^\circ\text{N}$) with $\sigma > 0.15 \text{ km}^{-1}$, in contrast to the low aerosol loading over the equatorial regions. In general, near-surface aerosol extinction is highest at $\sim 0.5 \text{ km}$ with σ upto 0.2 km^{-1} , however comparable aerosol loading persists through 4 km with some measurable aerosol extinction within

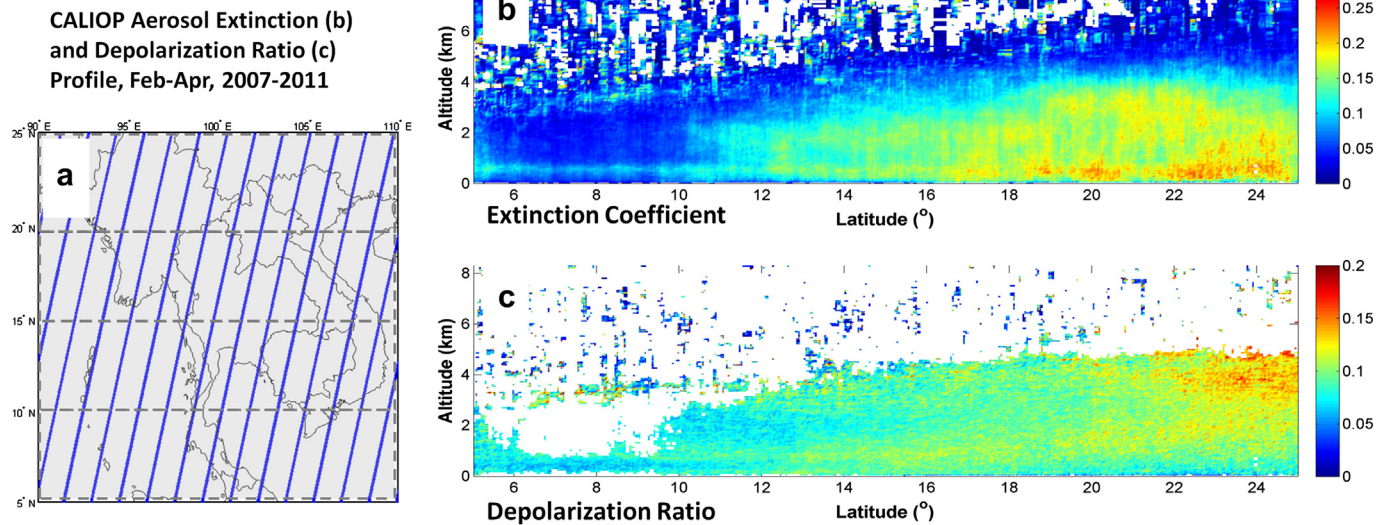


Fig. 2. CALIOP aerosol extinction and depolarization ratio profile measurements averaged over the Indochina peninsula domain, where (a) each blue line represents about 40 overlapping CALIOP tracks (with 608 total tracks available) for the February–April, 2007–2011 period, (b) latitudinal mean aerosol extinction profile (km⁻¹), and (c) depolarization ratio, from 5°N to 25°N. (For interpretation of the references to color in this figure legend, the reader is referred to the web version of this article.)

4–5 km layer ($0.05 < \sigma < 0.09 \text{ km}^{-1}$), in contrast to the equatorial regions.

In terms of particle shape/size, the zonal mean depolarization ratio (Fig. 2c) shown in similar fashion as the extinction coefficient, suggests bulk of the smoke-laden aerosol concentration dominated by spherical particles (e.g., organic carbon, sulfate, black carbon, etc.), associated with small VDR values ($<10\%$) in the vertical domain. Although smoke and pollution aerosols contain non-spherical soot as well, the depolarization ratio for these aerosol types is normally low because of the small size of soot particles and frequent internal inclusion of soot within organic carbon aerosols. Based on CALIOP data, Liu et al. (2008) classified VDR into several smoke and dust prevalent regions. For example, for central and southern African smoke, VDR values were generally found to be smaller than 6% with a typical value of 2–3%, while higher values were reported for Saharan dust in the 15–30% range (Liu et al., 2008). On the other hand, over the northern regions of Southeast Asia from 22°N to 25°N, increased non-spherical particulate concentration is found, as suggested by higher VDR values of $\sim 15\%$ located in the free troposphere within 2–4 km. One possibility of this greater non-spherical contribution could be due to long-range dust

transport from India associated with westerly flow during March–April (as suggested by air mass trajectory simulations, not shown here). The observed VDR over the northern region ($\sim 15\%$) is relatively smaller than that over other heavy dust-laden regions (15–30%) and therefore represents a well mixed state of spherical and non-spherical particles in the free troposphere relative to near surface and boundary layer conditions (Fig. 2c). This observation of possibly greater dust fraction is noteworthy as it adds to the complexity of aerosols in the smoke-laden region and may influence aerosol optical properties, however the noted higher VDR and its attribution requires further investigation in a separate work. It is also important to note that, in this analysis, VDR values were filtered out for small aerosol extinction retrievals (low aerosol loading conditions) in order to minimize bias due to low confidence retrievals (by setting a threshold on aerosol extinction as 0.05 km^{-1}).

3.3. Aerosol optical properties

As discussed previously in Section 2.1, the aerosol optical properties data obtained from the AERONET sunphotometers were used for studying ASD and SSA during the spring season. Table 1

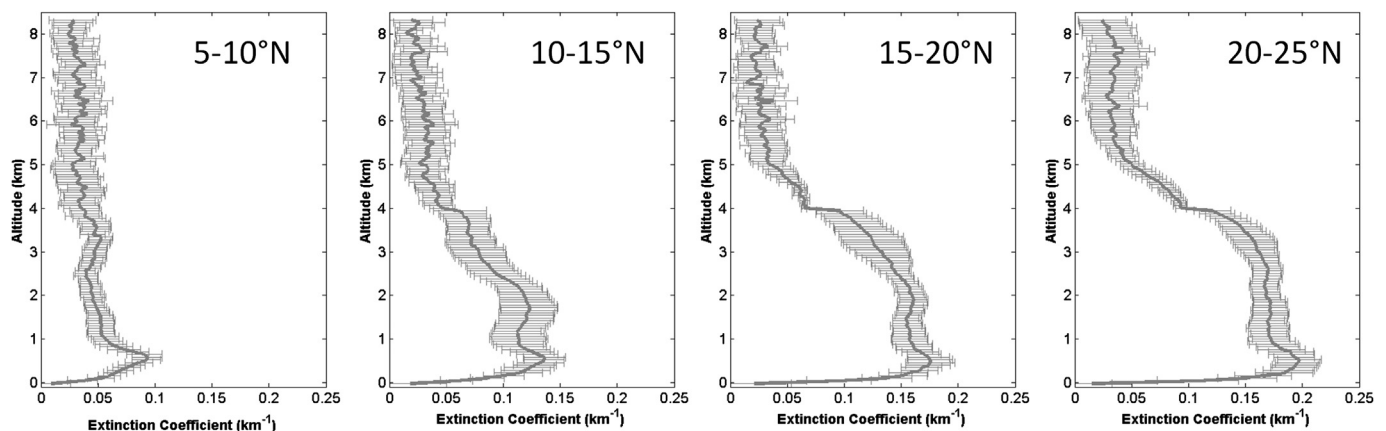


Fig. 3. Zonal mean CALIOP aerosol extinction profile for the February–April, 2007–2011 period, indicating variations in aerosol vertical distribution for the 4 sub-regions of Indochina (dashed boxes shown in Fig. 2a) from south to north (separated by a 5° interval).

Table 1

The site information of AERONET stations at Chiang Mai, Mukdahan, Phimai and Silpakorn University and time period of the data analyzed. Seasonal mean values (and 1 standard deviation) of AOD and AE (440 nm–870 nm) are also shown for each location corresponding to the pre-monsoon period.

Site information	Period	Aerosol optical depth	Angstrom exponent
Chiang Mai Met Sta (18.77°N, 98.97°E, 312 masl)	Feb–Apr, 2008–2009	0.8 ± 0.41	1.54 ± 0.2
Mukdahan (16.60°N, 104.67°E, 166 masl)	Feb–Apr, 2006–2009	0.58 ± 0.3	1.51 ± 0.22
Phimai (15.18°N, 102.56°E, 220 masl)	Feb–Apr, 2006–2008	0.56 ± 0.28	1.51 ± 0.21
Silpakorn University (13.81°N, 100.04°E, 72 masl)	Feb–Apr, 2007–2010	0.55 ± 0.27	1.43 ± 0.27

lists the site information along with the time period for which the data are analyzed. As can be seen from the seasonal mean Angstrom Exponent (AE) at 440–870 nm, typically above 1.4 at all sites, a strong presence of fine-mode pollution is evident, associated with smoke activity and urban aerosols. However, it is noted that these Angstrom exponents are lower than for regions that are dominated purely by biomass burning such as southern Africa (Eck et al., 2003) and Amazonia (Schafer et al., 2008), where AE values exceed ~1.7 for peak burning season months. Seasonal mean ASD and SSA, from almucantar retrievals obtained from the sky radiance measurements, are presented in Fig. 4 for all 4 sites, thus covering a broad region in Thailand. In order to focus on fine-mode pollution aerosols, almucantar retrievals were filtered out for cases when AE < 1 and then averaged to represent seasonal mean. A typical bimodal lognormal size distribution is seen in the seasonal mean at all sites with a dominant fine-mode peak. The fine-mode is consistently observed with a peak centered at 0.14 μm radius for all locations with the strongest fine-mode ($0.12 \mu\text{m}^3 \mu\text{m}^{-2}$) observed in the northern regions of Thailand at Chiang Mai, followed by over Mukdahan. Here, the seasonal mean ASD and SSA is only shown for moderate-to-high aerosol loading conditions (AOD at 440 nm > 0.4), in order to screen out low confident retrievals from the analysis. The pronounced fine-mode peak is also consistent with large fine-fraction AOD comprising over 80% of the total AOD compared to small coarse-fraction AOD (<0.1) during pre-monsoon period, as suggested by the AERONET-derived inversion product (see Supplementary Fig. S2). It is worth pointing out that, in addition to the prominent fine-mode peak in the size distribution, all sites are also associated with a non-negligible coarse mode during

the pre-monsoon season. One of the major possibilities for the coarse mode peak could be attributed to contribution by soil-type aerosols locally emitted from dry agriculture croplands (e.g. over Phimai) or even from urban/construction activities (e.g., over Chiang Mai). For example, insitu data analysis over Phimai has indicated a measurable (~20–25%) coarse mode fraction of the total volume aerosol concentration largely from local soil particulates (Li et al., 2013). Other factors contributing to the coarse mode possibly include long-range transport of mineral dust from India as suggested by air mass trajectory simulations ending over Indochina peninsula, especially over northern regions (not shown). There could also be some residual cirrus cloud contamination influencing the size distribution retrievals as previously shown by Huang et al. (2011). However, the cirrus cloud frequency and potential bias to aerosol retrievals is more likely during the monsoon period i.e., from May onwards with relatively less likelihood of contamination (Huang et al., 2011) during the pre-monsoon season, i.e. focus period of our study.

In terms of aerosol absorption, the spectral SSA indicates a typical negative gradient with respect to increasing wavelengths, which suggest a mixture of fine mode dominated organic carbon, water soluble and black carbon aerosols (more scattering at shorter wavelengths i.e., 440 and 670 nm and greater absorption at longer wavelengths i.e., 870 and 1020 nm). In general, the aerosol loading for all locations is found to be quite absorbing with the spectral SSA less than 0.91 at all wavelengths. Among the 4 sites, Chiang Mai represents the most absorbing aerosol type with the spectral SSA less than 0.85 at all wavelengths associated with a steep slope. On the other hand, the spectral SSA is relatively flat over Phimai and also suggests presence of more scattering aerosol compared to other regions. Thus, based on the relative aerosol optical/radiative characteristics, the two locations, i.e. Chiang Mai in the north and Phimai in south, show extreme behavior due to a number of factors. Foremost is the fact that Chiang Mai is an urban city with heavy pollution and affected strongly by biomass burning emissions due to its close proximity to the forested regions near the Thai–Myanmar border. The valley-type topography of Chiang Mai surrounded by mountains favors aerosol build up associated with trapping of pollutants near-surface. Furthermore, analysis of PM₁₀ concentrations at several locations in Thailand indicates generally higher pollution levels in Chiang Mai (northern Thailand) compared to other regions including central Thailand (e.g., Phimai) as well as the Bangkok metropolitan area (Li et al., 2013). Thus, local urban/industrial emissions with forest fire/biomass burning smoke prevalent in the northern regions suggest the possibility of

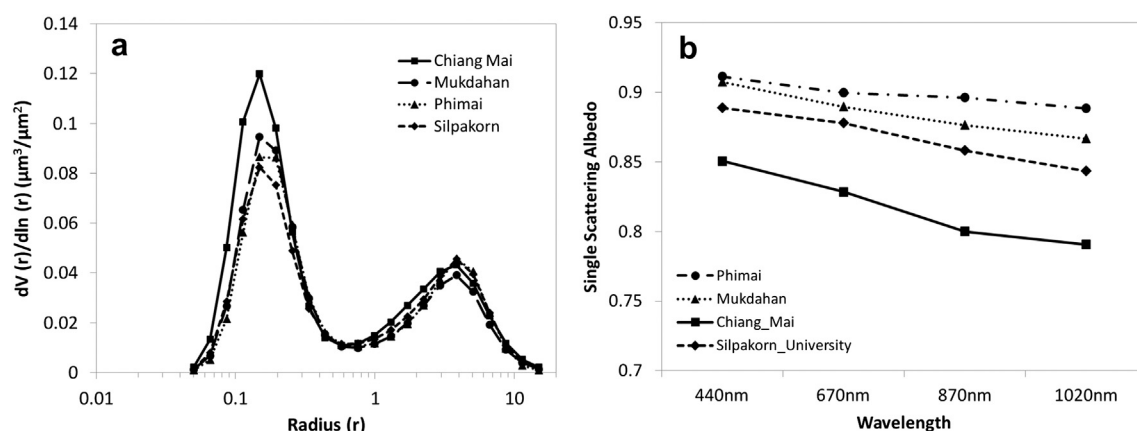


Fig. 4. Column-integrated aerosol optical properties from AERONET sunphotometer measurements at four locations distributed over Thailand: seasonal mean (Feb–Apr) ASD (a) and SSA (b) at Phimai (Feb–Apr, 2008–09), Mukdahan (Feb–Apr, 2006–2009), Chiang Mai (Feb–Apr, 2006–2008) and Silpakorn University (Feb–Apr, 2007–2010).

enhanced absorbing aerosol concentrations leading to lower SSA, as observed over Chiang Mai.

3.4. Aerosol daytime variability

Next, we investigate daytime variability patterns in aerosol loading from direct-sun measurements over the AERONET sites. As a pre-processing and sanity check, AOD retrievals with $AE > 1.2$ are considered for analysis in order to focus on fine-mode aerosols and also to avoid potential cloud/cirrus contamination in the retrievals (Huang et al., 2011) that may introduce biases in our daytime variability assessment. The methodology for analyzing daytime variations in aerosol loading is similar to previous works by Smirnov et al. (2002), Wang et al. (2004), Gautam et al. (2011). Difference between all instantaneous measurements, for a given day, from the respective daily mean is taken to represent the AOD departures, followed by averaging the departures in hourly intervals. This scheme allows us to systematically study daytime variability and helps in identifying patterns/trends in aerosol loading on an hourly scale. Similar procedure was applied to water vapor and AE data from the sunphotometer data. This procedure is applied to the direct sun measurements for the peak smoke-laden period (March–April) for two coinciding years 2008 and 2009 over Chiang Mai, Mukdahan and Silpakorn University. Over Phimai, data for March–April from years 2007 and 2008 are used in the analysis, as AERONET measurements from 2008 onwards are not available at Phimai.

Fig. 5 shows the resulting daytime variability patterns for AOD, AE and water vapor for Chiang Mai, Silpakorn and Phimai. The sample size, corresponding to the number of direct sun measurements (averaged for every hour) indicated as count, is also shown in Supplementary Fig. S3. A strong daytime pattern is observed over Chiang Mai with over 18% difference in the AOD departure between the peak early morning hours (7:30–9:30) and low mid-afternoon hours (13:30–15:30). A general cyclical pattern is found over Chiang Mai with aerosol loading peaking through early morning followed by a gradual and steady decrease from forenoon through afternoon and an increasing trend in the late afternoon/evening period. Variations in water vapor loading also show similar pattern, although to a lesser magnitude, suggesting changes in boundary layer evolution with higher moisture availability in early morning compared to afternoon hours. Difference of $\sim 7\%$ is found in water vapor loading between peak/low hours. In terms of variability in particle size (as shown by AE), changes are not as pronounced as compared to aerosol loading, but generally indicate the presence of greater particle size in the morning hours relative to late afternoon.

Similarly, measurements from the AERONET site at Silpakorn University also show a significant daytime variability in aerosol loading with a peak difference of more than 20% amplitude in AOD. Over Phimai, located in central rural Thailand, AOD variability also exists during daytime with about 15% departure observed from morning to afternoon. Data from Mukdahan show relatively smaller diurnal variability pattern (not shown), within 4–5%, but associated with similar slightly higher AOD departure and larger particle size variations during morning hours.

One of the possibilities rendering diurnal patterns in biomass burning regions may be associated with smoke transport through the night thus causing diurnal maximum morning AODs. Forest fire-generated smoke from upwind regions of Amazonia have been suggested to cause enhanced early morning aerosol loading conditions over the downwind regions, based on AERONET data from the Alta Floresta site (Zhang et al., 2012). A similar transport phenomenon from upwind regions of higher fire counts (especially from forested regions in Myanmar) may be responsible in part for

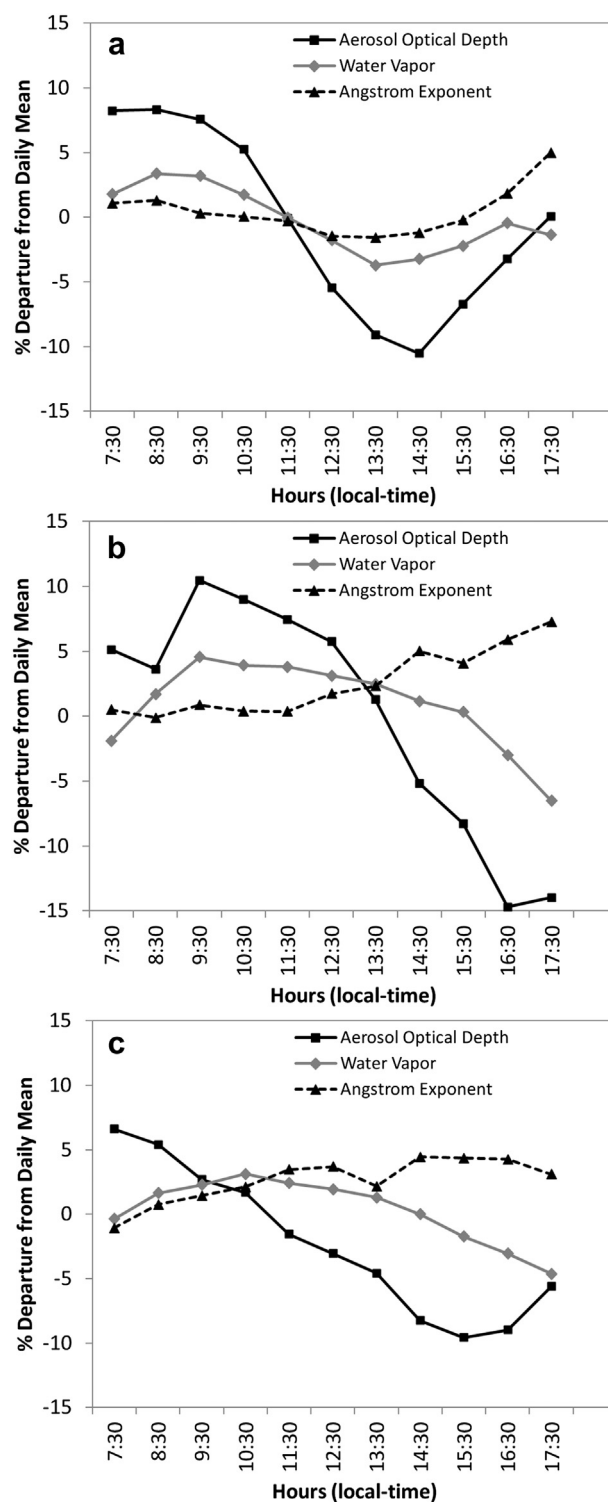


Fig. 5. Diurnal variability of AOD, water vapor and AE represented as percent departures from daily mean (averaged for every hour), obtained from AERONET sunphotometer direct sun measurements at (a) Chiang Mai (Mar–Apr, 2008–2009), (b) Silpakorn University (Mar–Apr, 2008–2009) and (c) Phimai (Mar–Apr, 2007–2008).

the morning maximum in AOD at the sites in Thailand. Other factors influencing the observed diurnal variability in aerosol loading may include diurnal cycle of fire activity, intensity and smoke transport patterns (Eck et al., 2003), which require further investigations of regional fire characteristics and emissions.

Furthermore, there are differences in the fine structure of daytime variability at the three locations in both amplitudes and timings of peak departures shown in Fig. 5. Such differences could be due to geographic location, local emission sources as well as boundary layer dynamics (Nodzu et al., 2006). For example, over Phimai, surface-based insitu data analysis indicates hygroscopic growth of aerosols during early morning due to high Relative Humidity conditions, relative to afternoon (Li et al., 2013). The wind field can be an important factor influencing the observed diurnal variability. For example, in the Bangkok Metropolitan area, near Silpakorn University, it has been previously shown that stagnant air flow, associated with low wind speed ($<5 \text{ m s}^{-1}$), favored accumulation of aerosols during early morning hours compared to increased wind speed during afternoon leading to increased horizontal dispersion of pollutants (Sahu et al., 2011). Thus, there are likely local factors that may also influence the long-range transport of smoke in causing the diurnal morning maximum. We therefore believe the diurnal variability pattern is a noteworthy observation and more investigation is required to better understand the observed characteristics in terms of continuous insitu measurements.

3.5. Direct aerosol radiative effect at TOA

In this section, we use CERES observations of TOA shortwave flux to derive instantaneous radiative effect at TOA in cloud-free conditions over selected AERONET locations. This observational approach allows us to determine the aerosol radiative forcing efficiency and also infer the absorbing nature of regional aerosol loading. The aerosol radiative forcing efficiency is defined as the change in direct shortwave flux per unit AOD, i.e., $\text{W m}^{-2}/\text{AOD}$. The efficiency is given by the slope of the linear regression between shortwave flux and AOD. The slope, which represents the efficiency at TOA (in this case), also indicates the absorbing nature of the column aerosol loading with smaller slope value suggesting increased aerosol absorption and vice versa. The offset is dominated by the underlying surface albedo that is a direct response of the varying surface types/albedo over

different regions shown. Previous studies have demonstrated the success and feasibility of using this approach for the estimation of aerosol forcing from satellite-derived TOA shortwave flux such as from the spaceborne Earth Radiation Budget Experiment (ERBE) and CERES sensors (Hsu et al., 2000; Zhang et al., 2005; Patadia et al., 2008).

We analyze the co-located CERES TOA flux with MODIS AOD in the SSF product for the 3-month period from February to April for two years – 2008 and 2009. The spatial resolution of each SSF pixel is $20 \text{ km} \times 20 \text{ km}$ at nadir; and the TOA flux data were gridded into a uniform spatial resolution of $0.25^\circ \times 0.25^\circ$ format. The co-located aerosol-flux dataset represents cloud-free conditions, however to avoid any potential residual cloud contamination (due to relatively larger pixel size of CERES), we utilize the co-located cloud fraction information (from the same platform) in the SSF product to further screen the flux data. A stringent cloud-screening scheme is employed to minimize cloud contamination with CERES pixels associated with cloud fraction higher than 0% being filtered out and not considered for further analysis. This screening may possibly reject heavy aerosol loading cases from our analysis, however it allows us to avoid potential artifacts and therefore reduce biases/uncertainties associated with the forcing analysis. It is also important to point out that this observational approach, involving satellite-retrieved shortwave fluxes and AOD, is best suited for applications over oceanic and vegetated regions, i.e. over dark surfaces, where contribution of surface albedo to observed TOA radiance is small, thus allowing reliable aerosol radiative effect assessment. In order to ascertain the feasibility of the TOA-based radiative effect analysis, CERES-derived broadband surface albedo (Rutan et al., 2009) for the study region was used to verify the underlying surface effect. Fig. S4 (online supplementary figure) shows the composite mean map (and histogram) of broadband surface albedo for the February–April period with majority of the regions associated with albedo in the 0.12–0.16 range indicating low surface albedo over the largely vegetated regions.

The co-located aerosol loading – TOA flux dataset is analyzed over the AERONET locations in order to determine the regional forcing efficiency and to further compare aerosol absorption

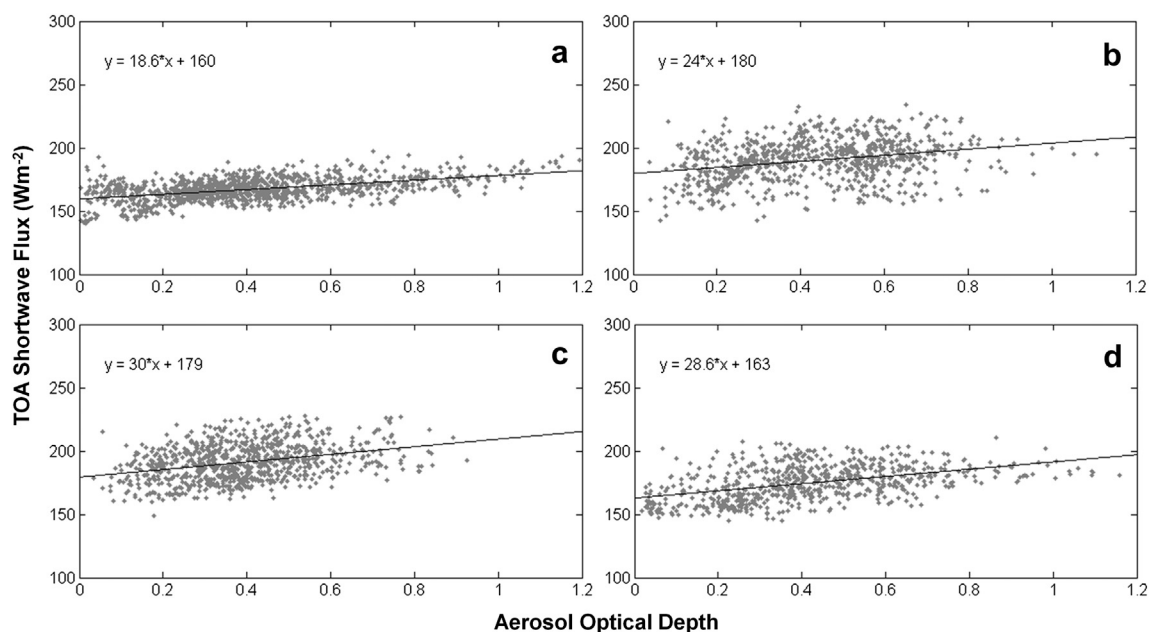


Fig. 6. Aerosol radiative forcing efficiency represented by the slope of linear regression between co-located CERES TOA shortwave flux and MODIS AOD observations averaged over selected $2^\circ \times 2^\circ$ regions, during February–April 2008–2009, centered over (a) Chiang Mai, (b) Mukdahan, (c) Phimai and (d) Silpakorn University.

characteristics, among different regions, from the radiation budget perspective. The gridded data are selected over a $2^\circ \times 2^\circ$ box centered over each AERONET site during the February–April period, constrained within the 25° – 35° solar zenith angle interval. Fig. 6 shows the CERES TOA flux from Terra co-located with MODIS AOD over (a) Chiang Mai, (b) Mukdahan, (c) Phimai, and (d) Silpakorn University. The instantaneous TOA forcing efficiency (F_e) varies from $18 \text{ W m}^{-2}/\text{AOD}$ to $30 \text{ W m}^{-2}/\text{AOD}$ over the four selected regions with the slope value smallest for Chiang Mai and largest for Phimai. The lower F_e over Chiang Mai is associated with enhanced aerosol absorption leading to less radiant energy being scattered at TOA (as a function of increasing aerosol loading) compared to other regions where the relative aerosol-induced scattering is larger, as indicated by the F_e values. This observation is consistent with the lower SSA (<0.85 for the 440 nm – 1020 nm wavelength range, Fig. 4) at Chiang Mai associated with its proximity to the northern forested regions near the Thai–Myanmar border where forest fire smoke is prevalent during the pre-monsoon season as well as due to generally higher urban pollution. In addition, the F_e over the Chiang Mai region is derived from a tight scatter of points ($r^2 = 0.5$) suggesting greater confidence in the observed radiative effect. On the other hand, aerosols over the Phimai region are relatively less absorbing as suggested by F_e that is consistent with the higher SSA values noted earlier for Phimai. The F_e values for Mukdahan ($28 \text{ W m}^{-2}/\text{AOD}$) and Silpakorn University ($28 \text{ W m}^{-2}/\text{AOD}$) are close to each other and fall within the extreme ends of the Chiang Mai–Phimai range of F_e , as also noted earlier in the case of SSA variations among the 4 locations. In contrast to the strong relationship between AOD and TOA shortwave flux observed over Chiang Mai, the forcing efficiency over Mukdahan region is derived from a relatively weak relationship which is most likely attributed to the heterogeneous surface type with mixed vegetation and bare soil surface types in the Mukdahan region, per visual inspection of visible imagery. Although regional aerosols are significantly absorbing, especially over Chiang Mai, overall the aerosol–TOA flux relationship results indicate that the regional aerosol layer is brighter than the underlying surface as it is associated with a positive slope (F_e), i.e. increasing TOA flux with respect to AOD and therefore induce negative forcing at TOA. Overall, a consistency in the aerosol-induced solar absorption characteristic is found among the selected regions from ground-based sunphotometer-derived spectral SSA retrievals and satellite-based radiative effect analysis at TOA.

4. Conclusions

The Indochina peninsular regions in Southeast Asia experience the earliest rainfall spells in late April–early May, signaling the onset of the Asian summer monsoon season over the inland regions. Prior to the monsoon onset, the extended dry pre-monsoon period witness intense biomass burning, in the form of forest fires and agricultural crop burning, with aerosol concentrations highest during this period on an inter-annual basis. In the context of the potential role of pre-monsoon aerosol loading in perturbing radiative energy balance and regional hydrological cycle, this paper focuses on aerosol distribution over the Indochina peninsula from an observational satellite-surface perspective, in order to better understand the regional aerosol characteristics in terms of aerosol optical properties, vertical distribution and radiative effects. Additionally, aerosols over the Southeast Asian region represent a complex mixture from urban and biomass burning sources, which undergo strong seasonal variation greatly influenced by the regional monsoon system, and therefore require improved characterization, radiative effect

assessment as well as validation of satellite-derived aerosol products (Janjai et al., 2005).

In general, the seasonal peak aerosol loading is strongly correlated with the biomass burning activity as indicated by inter-annual variations of AOD and fire count from MODIS data for the period 2001–2010. The pre-monsoon aerosol loading is also found to be associated with a strong north-south gradient from relatively clean equatorial environment to the more polluted regions of Myanmar and northern Thailand (15° – 25°N) associated with the biomass burning activity. In terms of vertical distribution, aerosol loading is largest near-surface and in the lower troposphere, however extends to elevated altitude ($\sim 4 \text{ km}$) over the northern regions as indicated by multi-year composite analysis of CALIOP aerosol extinction profile measurements. Both the CALIOP-derived depolarization ratio and ground-based sunphotometer data from AERONET stations indicate the dominance of widespread fine-mode smoke pollution in the vertically resolved and column-integrated measurements of aerosol optical properties (Angstrom Exponent, volume size distribution), respectively. Based on sunphotometer data obtained from four AERONET sites distributed over Thailand, a typical bi-modal lognormal size distribution is observed in the seasonal mean with a dominant fine-mode peak centered at $0.14 \mu\text{m}$ radius, for all locations, with the strongest fine-mode ($0.12 \mu\text{m}^3 \mu\text{m}^{-2}$) observed in the northern region of Chiang Mai, located in close proximity to the forested areas near the Thai–Myanmar border. The spectral SSA variations reflect on the strong influence of smoke aerosols and in general, suggest significant absorbing aerosol loading ($\text{SSA} < 0.91$ in the 440 – 1020 nm range), with the northern region of Chiang Mai characterized by most absorbing aerosol ($\text{SSA} \sim 0.85$ in the 440 – 1020 nm range) and the highest AOD. Strongly coupled to the stable pre-monsoon conditions associated with prominent inversion layer, the smoke-laden aerosol loading was further investigated in terms of diurnal variability and was found to exhibit significant pattern with higher AOD departures, in general, during early morning relative to late afternoon conditions (peak difference of 10 – 20%). Finally, satellite-based aerosol radiative impact is assessed using instantaneous CERES shortwave TOA flux, in conjunction with MODIS AOD, that also indicate significant absorbing aerosol loading over the northern region, with forcing efficiency (F_e) of $19 \text{ W m}^{-2}/\text{AOD}$ at Chiang Mai (in the 25° – 35° solar zenith angle range). Overall, a consistency in the aerosol-induced solar absorption characteristic is found among the selected regions from ground-based sunphotometer-derived spectral SSA retrievals and satellite-based radiative effect analysis at TOA.

Acknowledgments

This work is supported by grant from the NASA Radiation Sciences Program, managed by Hal B. Maring. We thank the various science teams for provision of satellite data namely, CALIPSO, CERES and MODIS. The authors also gratefully acknowledge the efforts made by the AERONET team and site managers, including Jariya Boonjawat (Phimai) and Surasak Meesiri (Mukdahan), in maintaining the sites and making the data available online. We also thank Jingfeng Huang, Can Li, Zhaoyan Liu, Falguni Patadia for helpful discussions during preparation of the manuscript. Two anonymous reviewers are thanked for providing useful comments that helped improve an earlier version of the manuscript.

Appendix A. Supplementary material

Supplementary material associated with this article can be found, in the online version, at <http://dx.doi.org/10.1016/j.atmosenv.2012.05.038>.

References

- Carmichael, G.R., Ferm, M., Thongboonchoo, N., Woo, J.-H., Chan, L.Y., Murano, K., Viet, P.H., Mossberg, C., Bala, R., Boonjawat, J., Upatum, P., Mohan, M., Adhikary, S.P., Shrestha, A.B., Pienaar, J.J., Brunke, E.B., Chen, T., Jie, T., Guoan, D., Peng, L.C., Dhiharto, S., Harjanto, H., Jose, A.M., Kimani, W., Kirouane, A., Lacaux, J.-P., Richard, S., Barturen, O., Carrasco Cerda, J., Athayde, A., Tavares, T., Cotrina, J.S., Bilici, E., 2003. Measurements of sulfur dioxide, ozone and ammonia concentrations in Asia, Africa, and South America using passive samplers. *Atmospheric Environment* 37, 1293–1308.
- Chew, B.N., Chang, C.W., Liew, S.C., Salinas, S.V., 2008. Remote sensing measurements of aerosol optical thickness and correlation with in-situ air quality parameters during a biomass burning episode in Southeast Asia. In: *Proceedings of the 29th Asian Conference on Remote Sensing (ACRS2008)* 10–14 November 2008, Colombo, Sri Lanka, Paper no. TS25.4.
- Eck, T.F., Holben, B.N., Reid, J.S., Dubovik, O., Smirnov, A., O'Neil, N.T., Slutsker, I., Kinne, S., 1999. Wavelength dependence of the optical depth of biomass burning, urban, and desert dust aerosols. *Journal of Geophysical Research* 104, 31333–31349.
- Eck, T.F., Holben, B.N., Ward, D.E., Mukelabai, M.M., Dubovik, O., Smirnov, A., Schafer, J.S., Hsu, N.C., Piketh, S.J., Queface, A., Le Roux, J., Swap, R.J., Slutsker, I., 2003. Variability of biomass burning aerosol optical characteristics in southern Africa during the SAFARI 2000 dry season campaign and a comparison of single scattering albedo estimates from radiometric measurements. *Journal of Geophysical Research* 108, 8477. <http://dx.doi.org/10.1029/2002JD002321>.
- Gautam, R., Hsu, N.C., Tsay, S.C., Lau, K.M., Holben, B., Bell, S., Smirnov, A., Li, C., Hansell, R., Ji, Q., Payra, S., Aryal, D., Kayastha, R., Kim, K.M., 2011. Accumulation of aerosols over the Indo-Gangetic plains and southern slopes of the Himalayas: distribution, properties and radiative effects during the 2009 pre-monsoon season. *Atmospheric Chemistry and Physics* 11, 12841–12863. <http://dx.doi.org/10.5194/acp-11-12841-2011>.
- Holben, B.N., Eck, T.F., Slutsker, I., Tanre, D., Buis, J.P., Setzer, A., Vermote, E., Reagan, J.A., Kaufman, Y.J., Nakajima, T., Lavenu, F., Jankowiak, I., Smirnov, A., 1998. AERONET: a federated instrument network and data archive for aerosol characterization. *Remote Sensing of Environment* 66, 1–16.
- Hsu, N.C., Herman, J.R., Weaver, C., 2000. Determination of radiative forcing of Saharan dust using combined TOMS and ERBE data. *Journal of Geophysical Research* 105, 20,649–20,661.
- Hsu, N.C., Herman, J.R., Tsay, S., 2003. Radiative impacts from biomass burning in the presence of clouds during boreal spring in Southeast Asia. *Geophysical Research Letters* 30 (5), 1224.
- Huang, J., Hsu, N.C., Tsay, S.-C., Jeong, M.-J., Holben, B.N., Berkoff, T.A., Welton, E.J., 2011. Susceptibility of aerosol optical thickness retrievals to thin cirrus contamination during the BASE-ASIA campaign. *Journal of Geophysical Research* 116, D08214. <http://dx.doi.org/10.1029/2010JD014910>.
- Janjai, S., Laksanaboonsong, J., Nunez, M., Thongsathitya, A., 2005. Development of a method for generating operational solar radiation maps from satellite data for a tropical environment. *Solar Energy* 78, 739–751.
- Janjai, S., Suntaropas, S., Nunez, M., 2009. Investigation of aerosol optical properties in Bangkok and suburbs. *Theoretical and Applied Climatology* 96, 221–233.
- Lau, K.-M., Yang, S., 1997. Climatology and interannual variability of the southeast Asian summer monsoon. *Advances in Atmospheric Sciences* 14, 141–162.
- Lau, K.M., Kim, M.K., Kim, K.M., 2006. Asian monsoon anomalies induced by aerosol direct effects. *Climate Dynamics* 26, 855–864.
- Levy, R.C., Remer, L.A., Mattoo, S., Vermote, E.F., Kaufman, Y.J., 2007. Second-generation operational algorithm: retrieval of aerosol properties over land from inversion of Moderate Resolution Imaging Spectroradiometer spectral reflectance. *Journal of Geophysical Research* 112, D13211. <http://dx.doi.org/10.1029/2006JD007811>.
- Li, C., Tsay, S.C., Hsu, N.C., Kim, J.Y., Howell, S.G., Huebert, B.J., Ji, Q., Jeong, M.J., Wang, S.H., Hansell, R.A., Bell, S.W., 2013. Characteristics and Composition of Atmospheric Aerosols in Phimai, Central Thailand during BASE-ASIA. *Atmospheric Environment* 78, 60–71.
- Liu, Z., Liu, D., Huang, J., Vaughan, M., Uno, I., Sugimoto, N., Kittaka, C., Trepte, C., Wang, Z., Hostetler, C., Winker, D., 2008. Airborne dust distributions over the Tibetan Plateau and surrounding areas derived from the first year of CALIPSO lidar observations. *Atmospheric Chemistry and Physics* 8, 5045–5060.
- Loeb, N.G., Kato, S., 2002. Top-of-atmosphere direct radiative effect of aerosols from the Clouds and the Earth's Radiant Energy System Satellite instrument (CERES). *Journal of Climate* 15, 1474–1484.
- Nodzu, M.I., Ogino, S., Tachibana, Y., Yamanaka, M.D., 2006. Climatological description of seasonal variations in lower tropospheric temperature inversions layers over the Indochina Peninsula. *Journal of Climate* 19, 3307–3319.
- Patadia, F., Gupta, P., Christopher, S.A., Reid, J.S., 2008. A Multisensor satellite-based assessment of biomass burning aerosol radiative impact over Amazonia. *Journal of Geophysical Research* 113, D12214. <http://dx.doi.org/10.1029/2007JD009486>.
- Pengchai, P., Chantara, S., Sopajaree, K., Wangkarn, S., Tengcharoenkul, U., Rayanakorn, M., 2009. Seasonal variation, risk assessment and source estimation of PM 10 and PM10-bound PAHs in the ambient air of Chiang Mai and Lamphun, Thailand. *Environmental Monitoring Assessment* 154, 197–218.
- Ramanathan, V., Crutzen, P.J., Kiehl, J.T., Rosenfeld, D., 2001. Atmosphere – aerosols, climate, and the hydrological cycle. *Science* 294 (5549), 2119–2124.
- Ramanathan, V., Chung, C., Kim, D., Bettge, T., Buja, L., Kiehl, J.T., Washington, W.M., Fu, Q., Sikka, D.R., Wild, M., 2005. Atmospheric brown clouds: impacts on South Asian climate and hydrological cycle. *PNAS* 102, 5326–5333.
- Rutan, D., Rose, F., Roman, M., Manalo-Smith, N., Schaaf, C., Charlock, T., 2009. Development and assessment of broadband surface albedo from clouds and the Earth's radiant energy system clouds and radiation swath data product. *Journal of Geophysical Research* 114, D08125. <http://dx.doi.org/10.1029/2008JD010669>.
- Schafer, J.S., Eck, T.F., Holben, B.N., Artaxo, P., Duarte, A.F., 2008. Characterization of the optical properties of atmospheric aerosols in Amazonia from long-term AERONET monitoring (1993–1995 and 1999–2006). *Journal of Geophysical Research* 113, D04204. <http://dx.doi.org/10.1029/2007JD009319>.
- Sahu, L.K., Kondo, Y., Miyazaki, Y., Pongkiatkul, P., Kim Oanh, N.T., 2011. Seasonal and diurnal variations of black carbon and organic carbon aerosols in Bangkok. *Journal of Geophysical Research* 116. <http://dx.doi.org/10.1029/2010JD015563>.
- Smirnov, A., Holben, B.N., Eck, T.F., Slutsker, I., Chatenet, B., Pinker, R.T., 2002. Diurnal variability of aerosol optical depth observed at AERONET (Aerosol Robotic Network) sites. *Geophysical Research Letters* 29, 2115.
- Streets, D.G., Yan, F., Chin, M., Diehl, T., Mahowald, N., Schultz, M., Wild, M., Wu, Y., Yu, C., 2009. Anthropogenic and natural contributions to regional trends in aerosol optical depth, 1980–2006. *Journal of Geophysical Research* 114. <http://dx.doi.org/10.1029/2008JD011624>.
- Wang, J., Xia, X., Wang, P., Christopher, S.A., 2004. Diurnal variability of dust aerosol optical thickness and Angstrom exponent over dust source regions in China. *Geophysical Research Letters* 31. <http://dx.doi.org/10.1029/2004GL019580>.
- Wielicki, B.A., Barkstrom, B.R., Harrison, E.F., Lee, R.B., Smith, G.L., Cooper, J.E., 1996. Clouds and the Earth's Radiant Energy System (CERES): an Earth observing system experiment. *Bulletin of American Meteorological Society* 77, 853–868.
- Winker, D.M., Pelon, J., Coakley Jr., J.A., Ackerman, S.A., Charlson, R.J., Colarco, P.R., Flamant, P., Fu, Q., Hoff, R., Kittaka, C., Kubar, T.L., LeTreut, H., McCormick, M.P., Megie, G., Poole, L., Powell, K., Trepte, C., Vaughan, M.A., Wielicki, B.A., 2010. The CALIPSO mission: a global 3-D view of aerosols and clouds. *Bulletin of American Meteorological Society* 91, 1211–1229. <http://dx.doi.org/10.1175/2010BAMS3009.1>.
- Zhang, J., Christopher, S.A., Remer, L.A., Kaufman, Y.J., 2005. Shortwave aerosol radiative forcing over cloud-free oceans from Terra: 2. Seasonal and global distributions. *Journal of Geophysical Research* 110, D10S24.
- Zhang, Y., Yu, H., Eck, T.F., Smirnov, A., Chin, M., Remer, L.A., Bian, H., Tan, Q., Levy, R., Holben, B.N., Piazzolla, S., 2012. Aerosol daytime variations over North and South America derived from multiyear AERONET measurements. *Journal of Geophysical Research* 117. <http://dx.doi.org/10.1029/2011JD017242>.